

Bird's-Eye View to Street-View: A Survey

Khawlah Bajbaa, Muhammad Usman*, Saeed Anwar, Ibrahim Radwan, and Abdul Bais

Abstract—In recent years, street view imagery has grown to become one of the most important sources of geospatial data collection and urban analytics, which facilitates generating meaningful insights and assisting in decision-making. Synthesizing a street-view image from its corresponding satellite image is a challenging task due to the significant differences in appearance and viewpoint between the two domains. In this study, we screened 20 recent research papers to provide a thorough review of the state-of-the-art of how street-view images are synthesized from their corresponding satellite counterparts. The main findings are: (i) novel deep learning techniques are required for synthesizing more realistic and accurate street-view images; (ii) more datasets need to be collected for public usage; and (iii) more specific evaluation metrics need to be investigated for evaluating the generated images appropriately. We conclude that, due to applying outdated deep learning techniques, the recent literature failed to generate detailed and diverse street-view images.

Index Terms—Computer Society, IEEE, IEEEtran, journal, L^AT_EX, paper, template.

I. INTRODUCTION

GENERATING street-view images from satellite-view is one of the rising topics in the cross-view image translation domain. It aims to generate geometrically consistent street views corresponding to the center-located area on the provided satellite view. As satellite images are becoming more widely available (*e.g.*, Google Earth), it is becoming easier to cover almost every spot of the globe. However, such a capability does not exist for street-view images [1], as the majority of street-views are captured around known landmarks and major roads [2], [3]. It helps enhance the content in areas that are expensive or difficult to reach by people or vehicles. Also, street-view images enable more accurate geo-localization than satellite-view images.

Street-view synthesis is helpful for various downstream tasks, such as image geo-localization, which is considered a fundamental problem in many applications such as robotics, augmented reality, and autonomous driving [4]. The retrieval component is limited to identifying and locating similar objects, so adopting satellite to street-view synthesis plays a vital role in this task, where the generator can learn more valuable features that help in precise location retrieval. Moreover, street-view images have many additional useful details not in satellite images, like building facades [4]. Furthermore, cross-view matching between satellite and street views aids

K. Bajbaa, M. Usman and S. Anwar are with the Department of Information and Computer Science, King Fahd University of Petroleum and Minerals (KFUPM), Dhahran, Saudi Arabia. E-mail: {g202115030,muhammad.usman,saeed.anwar}@kfupm.edu.sa

M. Usman and S. Anwar are also with SDAIA-KFUPM Joint Research Center for Artificial Intelligence, KFUPM, Dhahran, Saudi Arabia.

I. Radwan is with the University of Canberra, Australian Capital Territory (ACT), Canberra, Australia.

A. Bais is with the University of Regina, Saskatchewan, Canada.

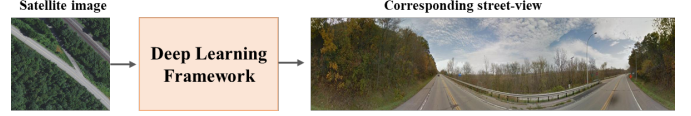


Fig. 1. General overview of satellite to street-view generation.

in predicting street-view segmentation maps based on satellite views of the same location for geo-orientation and geo-location estimation tasks by extracting features from a satellite image and mapping them into street-view, conveying semantics from street-view to satellite view [5]. Moreover, the representation derived from the conditional Generative Adversarial Networks (GANs) for generating street views from satellite images aids in distinguishing between rural and urban land covers. [6].

In recent years, synthesizing street-view from satellite images has been investigated by Generative Adversarial Network-based methods [7], [8], [6], [9], [4], or by combining U-Net [10] and BicycleGAN such as [1]. Differently, [11] and [8] explored the conditional GAN that learns the generation of both images, either street-view or satellite-view, and their corresponding semantic maps simultaneously. In addition, [12] and [13] investigated the semantic-guided cGAN where the semantic map concatenated with the input image. As a result, the semantic map serves as a guide to direct the model on generating images in another domain. On the other hand, street-view to satellite synthesis, has been explored by employing conditional GAN [14] for street-view geo-localization task for predicting street-view location. In addition, some other works investigated the street-view geo-localization task by matching it with satellite images using Convolutional Neural Networks (CNN) and feature matching-based methods [15], [2], Siamese Network [16], [17], [18], and Siamese and Triplet Network [19].

Figure 1 illustrates a general overview of the satellite to street-view generation. As a result of the challenging nature of this problem, it leaves an opportunity for further improvements. Despite the progress of satellite-to-street-view synthesis, it has limitations, as a satellite image only shows the top surface of an object. Therefore, it led to a hallucinatory representation of the facades of the objects. In addition, indistinguishable small objects such as cars, tree shadows, sidewalks, street lines, and fences are still being ignored in street-view synthesis.

II. BIRD EYE VIEW TO STREET VIEW METHODS

A. Conditional GAN-based Models

These methods share the commonality of utilizing conditional Generative Adversarial Networks (GANs) for image synthesis tasks. They are designed to generate realistic images

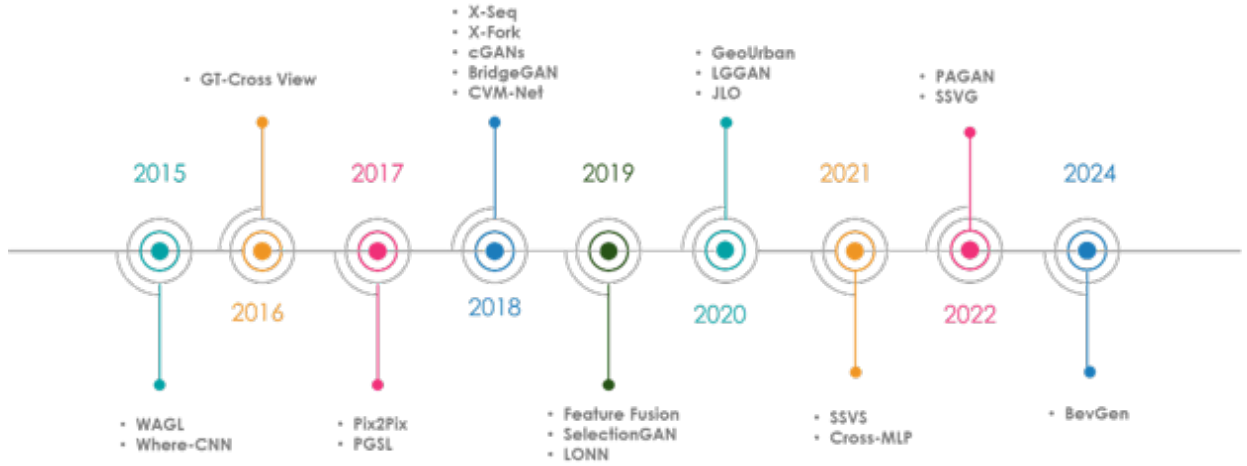


Fig. 2. Chronological display of the papers included in the survey. The chart illustrates the increasing trend towards deep models in the research evolving in the area of birds eye view to street view.

from different viewpoints or modalities, such as from bird’s eye to street view or vice versa. The focus is leveraging conditional information to produce high-quality images exhibiting desired characteristics.

1) *X-Fork* [11]: Regmi and Borji introduced two architectures based on conditional GANs called Cross-view Fork (X-Fork) and Sequential-view (Seq-X) for cross-image synthesis from street view to aerial view and vice versa. The X-Fork architecture used the baseline discriminator, where the generator network is forked, to produce segmentation maps and images, as shown in Figure 3(a). The Seq-X architecture uses two conditional GAN networks: the first network generates baseline cross-view images, which are fed to the second network as conditioning input to create the segmentation map in the same view, as illustrated in Figure 3(b). The results illustrated that X-Fork achieved higher accuracy with Top-1 and Top-5 for 64×64 resolution. On the other hand, X-Seq performed better with 256×256 resolution. This study employs two datasets: the first is the Dayton [19], and the second is the CVUSA.

2) *BEVGen* [20]: It proposed a conditional GAN-based model for generating realistic street-view images from Bird’s Eye View layout for traffic scenarios. The evaluation is conducted on the NuScenes 360 driving dataset [21]. Figure 3(c) shows an overview of BEVGen architecture, where it encoded both street-view images and BEV layout to latent discrete representation and flattened them for the autoregressive transformer. Subsequently, the spatial embeddings are added to the street view and Birds Eye View (BEV) tokens, and the pairwise bias is combined with the attention weight. After that, the decoder receives the tokens to get the generated street-view images. BEVGen compares with the baseline model, which has the same GPT architecture and uses identical first-stage encoders and decoders. The result indicates that BEVGen outperformed the baseline on metrics such as Fréchet Inception Distance (FID), road mIoU, and vehicle mIoU. As a limitation, BEVGen [20] faces challenges in accurately generating small objects like people and specific vehicles.

3) *GeoUrban** [1]: It exploits geometry to synthesize street-view images from satellite images. This study shows a 5km by 5km region of interest in the center of London City. The ground truth of depth and semantic satellite images is generated from stereo matching and supervised classification with post-correction. The architecture consists of three stages, as shown in Figure 3(d). The first is the satellite stage, which uses U-Net [10] to calculate a given satellite image’s depth and semantic images. The second stage is the geo-transformation stage, which converts the semantic and depth images of satellite images into their corresponding semantic and depth panorama images. The third stage, the street-view stage, is another U-Net [10] that refines the semantic panorama. Eventually, the BicycleGAN [22] is applied to generate realistic images from the semantic panorama. The novelty of the proposed method lies in offering a new transformation module for generating street-view images constrained by the geometric information of satellite images. Also, a novel weighted mask is utilized to mitigate the differences between the geometric panorama and satellite-depth images. The results demonstrated that the GeoUrban [1] outperformed other methods like Pix2Pix [23] and Regmi *et al.* [11]’s model with an accuracy of 72.9%.

4) *FeatureFusion* [14]: It takes advantage of conditional GANs to synthesize aerial images from ground-level panoramas. The X-Seq [11] is adopted with some modifications, such as reshaping the features into 2×2 and then performing different up-convolution operations to generate 512×512 aerial image resolution. The ground-level image and its edge-map are inputs to the X-Fork generator [11], as shown in Figure 3(e), which generates a synthesized aerial image and its corresponding edge-map. After that, FeatureFusion learns the joint feature representation of the ground-level image and the synthesized aerial image, and the features of the three images are integrated, followed by a fully connected layout to get a robust representation that matches the aerial feature representation. The novelty of the method lies in combining the edge map and semantic segmentation with input images

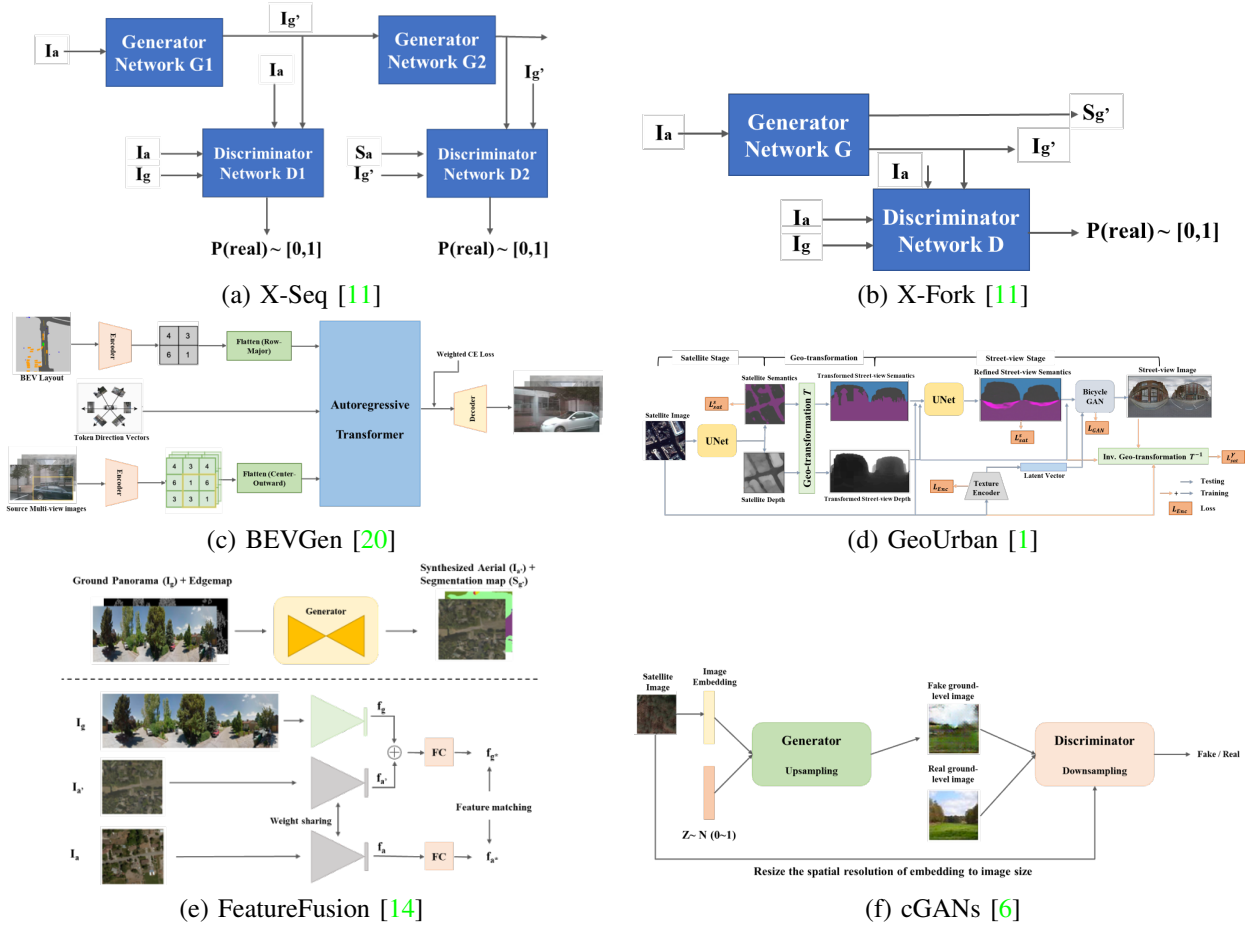


Fig. 3. Conditional GAN-based models.

to enhance the synthesis of cross-view. The results showed that the proposed feature fusion-based outperformed other approaches, including [2], [5], [19], [17] with 48.75% top-1 recall, 81.27% top-10 recall, and 95.98% top-1 accuracy. Moreover, FeatureFusion [14] experiments on the CVUSA and a new dataset the authors collected, the Orlando-Pittsburgh (OP) dataset.

5) *cGANs* [6]: use conditional GANs for generating ground-level images from satellite images and investigated cGANs feature maps for the land-cover classification. The satellite photos are collected via the Google Map Statistics API, while the ground-level images are taken from the Geograph API with known locations. The proposed framework addresses the problem of expressing an aerial picture’s information on how things appear on a ground-level image so that it can be used as input to the cGANs to generate ground-level photos. However, feeding 2D satellite image vectors to cGAN is ineffective due to the lack of structural similarity between satellite and ground-level images. Therefore, three types of image patch embedding are utilized to capture structural similarity: grayscale, HSV, and CNN. Figure 3(f) shows the proposed framework where the 1D image embedding vector is joined with a noise vector for the generator’s input. The feature maps generated by cGANs achieved the highest accuracy, with a value of 73.14%.

B. Multi Generator and Discriminator Models

As the name indicates, the multiple generator and discriminator models hierarchically employ many generators and discriminators.

1) *BridgeGAN* [24]: A multi-GAN model for generating bird-view images, BridgeGAN, introduces an intermediate view called the homography view to narrow the gap between the bird view and the frontal view. BridgeGAN consists of three GAN networks, as shown in Figure 4(a), each representing a specific view domain, namely homography-view, bird-view, and frontal-view. Each view domain has three components: a generator, a discriminator, and an encoder. In addition, shared layers are used to learn integrated intermediate representations since all three domains have the same semantic meaning. Cycle consistency loss consists of backward and forward cycles, while the introduced ResNet50 loss network imposes cross-view feature consistency. The novelty of BridgeGAN lies in addressing bird-view image generation from frontal-view images. The BridgeGAN achieves the best performance with values of 0.596 for SSIM, 5.01 for PSNR, and 0.242 for LPIPS compared with other baselines: Pix2Pix [23], cycleGAN [25], DiscoGAN [26], and CoGAN [27]. The dataset is obtained by collecting images from the Grand Theft Auto V video game using Palazzi *et al.*’s [28] framework.

2) *SelectionGAN* [13]: A multi-channel attention selection GAN comprises two stages for synthesizing images conditioned on the reference image and semantic map, as illustrated in Figure 4(b). The first stage focuses on the semantic features of the views, takes the target semantic map and the condition image (i.e., the ground-level image), and produces initial coarse results. The second stage targets the appearance details by refining the initial results via the multi-channel attention selection mechanism. The novelty lies in using coarse-to-fine inference to investigate cascaded semantic guidance. Moreover, a multi-attention module is offered to choose the intermediate generation attentively, which helps improve output quality. SelectionGAN [13] model is evaluated on three datasets: CVUSA [2] for aerial to ground-level images, Dayton [19] for ground-level to aerial images, and Ego2Top [29] (consists of pairs of two images of the same scene from two different views). The SelectionGAN achieved the best performance compared to pix2pix [23], X-Fork [11], X-Seq [11], and PGSL [5]. In some cases, on the CVUSA dataset, the X-Seq [11] occasionally performs slightly higher; however, SelectionGAN generates more realistic images.

3) *PAGAN* [8]: Progressive Attention GAN (PAGAN) has two primary components: a cross-stage attention module and a multi-stage progressive generation framework. Figure 4(c) shows an overview of the PAGAN, in which cross-stage attention is applied to generate a panorama through several coherent stages. PAGAN [8] comprises multiple segmentation and image generators for generating the street-view panorama and its segmentation map. In the first stage, the aerial image is fed to the image generator and segmentation generator, which produce the panorama and its corresponding segmentation map. After that, the generated image is refined by applying the cross-stage attention module, which forwards the semantic information stage by stage. The novelty of PAGAN lies in proposing a progressive generative framework for the high-resolution generation of street-view panoramas. Also, introducing a new cross-stage attention mechanism to bridge the subsequent generational stages allows the quality of street-view panoramas to improve continuously. The PAGAN outperformed other recent works: Pix2Pix [23], X-Fork [11], X-Seq [11], SelectionGAN [13], GAS2G [1], especially in terms of KL and FID scores, where the PAGAN reduced these scores significantly. In this study, two datasets are used, namely, the CVUSA and Orlando-Pittsburgh (OP) datasets.

4) *LGGAN* [12]: A Local class-specific and Global image-level GANs (LGGAN) model addresses semantic-guided-based scene generation tasks. LGGAN generation module is composed of three parts: a class-specific local generator for enriching the local scene details, an image-level global generator for capturing target images' overall structure and layout, and a weight-map generator for combining the resulted images from the global and local generators with the learned weight maps, as shown in Figure 4(d). The discriminator tries to differentiate generated images from semantic and image space. In addition, a new classification module is proposed to learn better discriminative class-specific feature representation. The novelty of LGGAN is that it considers

both local and global contexts. The LGGAN performs better on most evaluation metrics compared with other recent works, such as pix2pix [23], SelectionGAN [13], X-Seq [11], and X-Fork [11]. While SelectionGAN achieved slightly better performance on pixel-level metrics, i.e., PSNR, SD, and SSIM, than LGGAN. However, LGGAN generates more visually detailed objects like trees, buildings, and cars than SelectionGAN. The image translation part has been evaluated using the Dayton and CVUSA datasets.

C. Image-to-Image Translation Frameworks

Image-to-image translation frameworks operate on the premise of learning mappings between input and output images through supervised learning with paired data.

1) *Pix2Pix* [23]: A general framework that investigates using the conditional GAN for image-to-image translation. Though Pix2Pix [23] is not specific to bird-view to street-view, it has been extensively cited in this domain. The Pix2Pix [23] method is evaluated on many tasks and datasets: i) semantic labels to photos trained on Cityscapes [30], ii) map to aerial employs Google Map images, iii) edges to photo for [31] and [32], iv) sketch to photo for human sketches utilizing [33], and v) day to night using [34] data. The architecture of the generator and discriminator has been adapted from [35], where both are composed of Conv-BN-ReLU [36]. The skip connections are added to the generator, following the general shape of the U-Net [10], to allow low-level information from initial layers. Moreover, a novel discriminator, termed PatchGAN, penalizes structure at the image patch scale. The results showed that Pix2Pix [23] achieved the second-best result on the colorization task compared with Colorful Colorization [37], and a variant of their approach employed ℓ_2 regression [37]. Additionally, the Pix2Pix [23] model's aerial image generated from the map deceived the participants far more than the baseline. On the other hand, the generated map from an aerial image misled the participants by 6.1%, which is not substantially exceeding the baseline.

D. Semantic Feature Learning and Representation-based Models

These models prioritize extracting meaningful features from aerial photos and ground-level images, also called representations that capture essential semantic information. These representations serve as a compact and informative encoding of the input data, which can then be utilized for various downstream tasks. Representation learning involves training neural networks to learn features from raw image data automatically. The features are learned to capture relevant characteristics of the scenes depicted in the images, such as spatial layouts, object categories, textures, and other semantic information.

1) *PGSL** [5]: Zhai *et al.* presented a novel training technique for extracting meaningful features from aerial photos. The aim is to utilize the associated aerial image to predict the ground-level semantic layout. Four networks handle the features, as shown in Figure 5. The CNN network "A" extracts features from the aerial image via VGG16, and then it is fed to

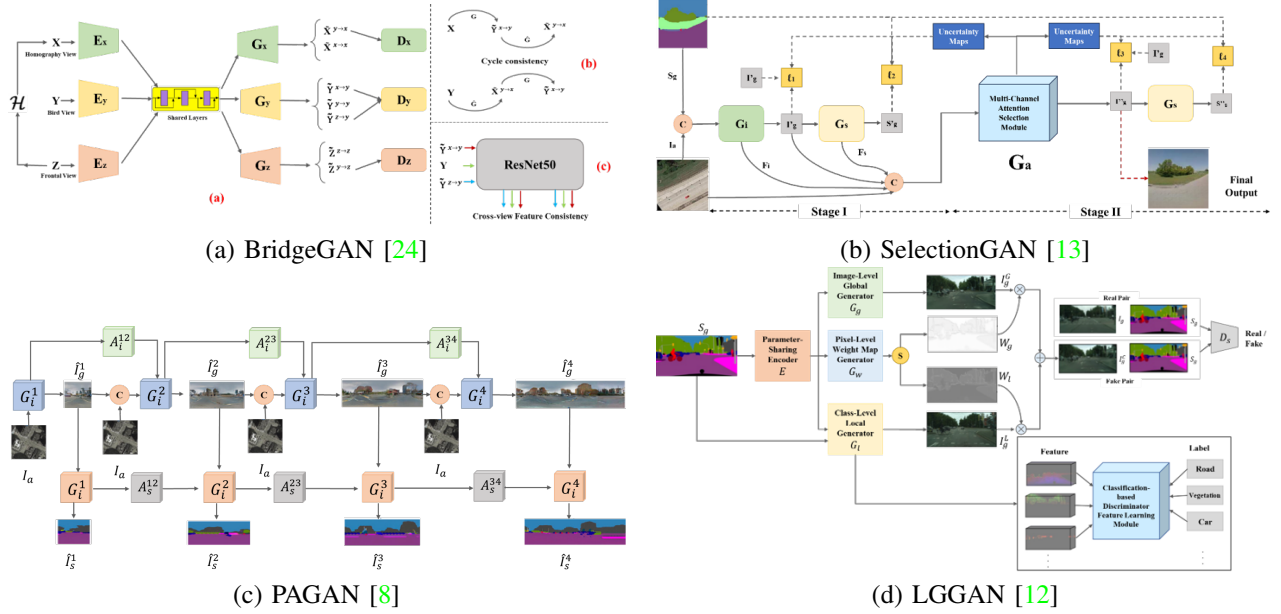


Fig. 4. Multi GAN-based models.

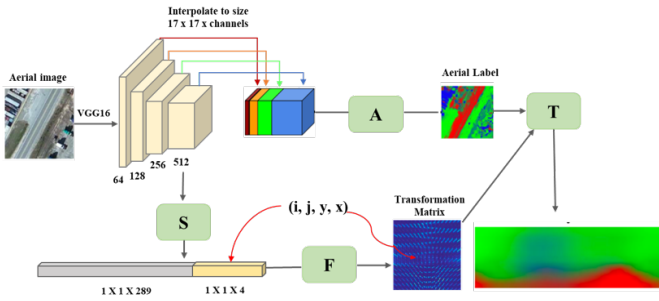


Fig. 5. PGSL* [5].

PixelNet [38] to convert it to pixel-level. The CNN network, “S”, employs the extracted features from aerial images to control the transformation. The network “F” estimates the change between viewpoints. Ground-level semantic labeling is created by applying the transformation, “T”, to the aerial semantic features. The novelty of this study lies in a new CNN design that links the appearance of an aerial image to a ground-level semantic layout located in the same location. Further, the PGSL [5] method can be extended to ground-level image orientation estimation, synthesis, and localization. Three different initializations have been experimented with: the proposed method initialization, Xavier [39] random initialization, and the VGG16 pre-trained on ImageNet initialization. The results demonstrated a superior performance of the proposed method compared to other initialization techniques on the CVUSA benchmark dataset.

2) *WAGL** [2]: Workman *et al.* address the wide-area geo-localization (WAGL) task employing pre-existing CNNs to extract the features from ground-level images and then learn to predict those features from the aerial photos with the exact location learning the semantic feature representation jointly. WAGL consists of two training models: a single-scale

model and a multi-scale model. The first model primarily aims to extract aerial features corresponding to ground-level images. The second model matches ground-level images to aerial photos at multiple spatial scales. The novelty lies in the in-depth analysis of existing CNN architectures for cross-view localization tasks with cross-view training for learning semantic features jointly from multiple image sources. The results showed that the features learned through multi-scale training outperformed single-scale and other methods [40], [41] on Charleston and San Francisco benchmark datasets.

E. Geometric Correspondence Models

The models in this group explicitly handle geometric correspondences between different views or modalities. They address the alignment of images based on known or learned geometric transformations, which is crucial for accurate information transfer and feature correspondence across domains. These methods ensure that the spatial relationships between images are preserved during synthesis or matching tasks.

1) *SSVS** [4]: It is a multi-task image synthesizing and retrieval architecture. SSVS stands for satellite-to-street view synthesis for geo-localization. The network learns the latent representations that are helpful for retrieval if they are employed for generating satellite and street-view images. In the proposed network, the generator is designed as U-Net [10], which consists of residual blocks, while the discriminator is constructed as a PatchGAN classifier [23]. The retrieval network consists of two main components, the encoder block and the spatial attention module, which convert an image’s local features into global representation, as illustrated in Figure 6(a). The results showed that the proposed method outperformed other models such as Pix2Pix [23], X-Fork [11], X-Seq [11], and PGSL [5] on CVUSA and CVACT datasets.

2) *SSVG** [7]: SSVG (Satellite and Street View Geometry) generates street-view images from satellite views based

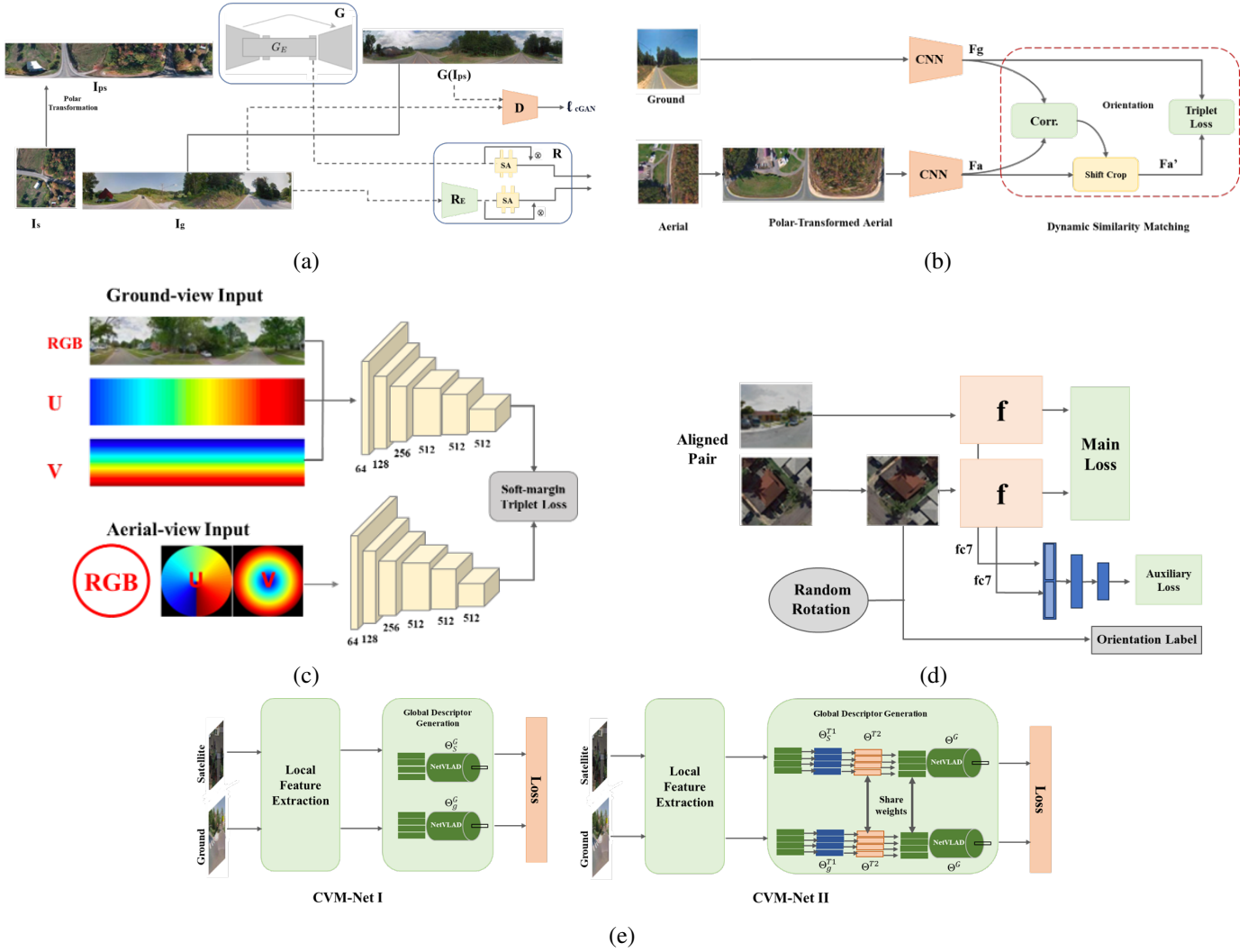


Fig. 6. Geometric correspondence models. (a) SSVS [4], (b) JLO [15], (c) LONN [18], (d) GT-CrossView [19], and (e) CVM-Net [17].

on modeling the geometric correspondences. Shi *et al.* [7] explicitly states the geometric correspondences between the satellite and street-view images, easing the information transfer between the mentioned domains. The proposed model applied the Satellite to Street-View Image Projection (S2SP) module to determine a geometric correspondence between street-view and satellite images. First, given the satellite image, the height probability is estimated through Pix2Pix [23], which is used for height estimation. Next, a satellite-view multiplane image (MPI) is constructed, given the satellite-view image and the estimated height probability distribution. Stretching and unrolling occur on each concrete cylinder to obtain a consistent street view. From street-view MPI, the final street-view image is generated in back-to-front order. Results are presented on two benchmark datasets: CVUSA [2] and CVACT [18] and illustrated that the SSVG [7] outperformed Pix2Pix [23] and X-Fork [11] on both the datasets.

3) *JLO* [15]: A recently proposed joint localization and orientation estimation method by Shi *et al.* [15] is based on Dynamic Similarity Matching (DSM) to measure the feature similarity of the image pair. The authors handle the cross-view

domain gap by using polar transform to align the aerial image up to an unknown azimuth angle, which helps the network learn the feature correspondences between polar aerial and ground images instead of having to learn the geometry relation between these two domains. Figure 6(b) shows an overview of the JLO method, where the polar transform is applied to an aerial image. Two stream-CNN networks are applied to extract polar-transformed aerial and ground-level image features. The orientation of the ground-level image concerning the aerial image is estimated using the correlation given the extracted feature volume representation. After that, the aerial features are shifted and cropped to get the image part that probably matches ground features, and the similarity is used for location retrieval. The novelty of this method is that it presents the first image-based geo-localization technique for estimating the orientation and position of ground-level images independent of their field of view. The JLO achieved the highest top-1 accuracy compared with other recent works [2], [5], [19], [17], [18], [14], with a value of 99.67% for CVUSA [2] and 97.32% for CVACT [18].

4) *LONN** [18]: stands for Lending Orientation to Neural Networks is a ground-level to aerial image matching method based on a Siamese network with explicit orientation encoding of each image pixel. The proposed method has been evaluated using the CVUSA benchmark dataset. In this study, Siamese-type two-branch CNN has been applied, where each branch will learn the useful features for comparing the views. The understanding of an image’s orientation facilitates the localization task, and based on that; the authors presented a method for injecting the orientation information for each pixel via orientation maps. Figure 6(c) shows an overview of the LONN [18], where ground-level and aerial images are fed to the Siamese network along with their associated orientation maps. The triplet loss function receives the two learned feature vectors and uses them to train the network. The orientation map injection can be done in two ways: either concatenated with the input layer only or injected in an intermediary convolution layer. The novelty of this work lies in proposing a simple approach for incorporating the orientation information of each pixel. Also, a novel Siamese-based CNN network is used to learn the feature embedding orientation and appearance information. The results showed that the proposed method outperformed other recent works Workman et al. [2], Zhai et al. [5], Vo et al. [19], and Hu et al. [17] with recall top-1 equal to 93.19%.

5) *GT-CrossView* [19]: : This model tackled ground-level to satellite image matching by investigating two categories of CNN networks. The first one is representation learning networks for embedding the cross-view images into the same feature space and classification networks for identifying matches. The second category is Siamese and triplet networks for computing similarity. A new Distance-Based Logistic Loss (DBL) function has introduced a novel version of Siamese and triplet networks. In this study, the orientation alignment is considered in addition to the spatial one, so learning the rotation invariant (RI) representation of satellite images helps learn complex representations without using more or larger filters and is done by simply applying random rotation to the training data, i.e., data augmentation. For better learning of representation, the authors proposed an auxiliary loss function where the added rotation amount can be utilized as a label. Figure 6(d) illustrates the network architecture that augments data through random rotation and incorporates an additional branch for orientation regression. The results demonstrate that both classification and hybrid (Siamese classification) networks performed better than feature representation networks, with an accuracy of 90% and 91.5%, respectively. Also, Siamese-DBL and triplet-DBL outperformed other original networks with accuracy rates of 88% and 90.2%, respectively. The images of a street view panorama are obtained by randomly querying the Google Map of the United States across 11 cities.

6) *CVM-Net* [17]: : It is an architecture for cross-view ground-to-aerial geolocation, consisting of two subnetworks, as shown in Figure 6(e). The first one, CVM-Net-I, contains two aligned NetVALDs layers that collect the local features into one common space from various views. The second one, CVM-Net-II, consists of two weight-shared NetVALDs

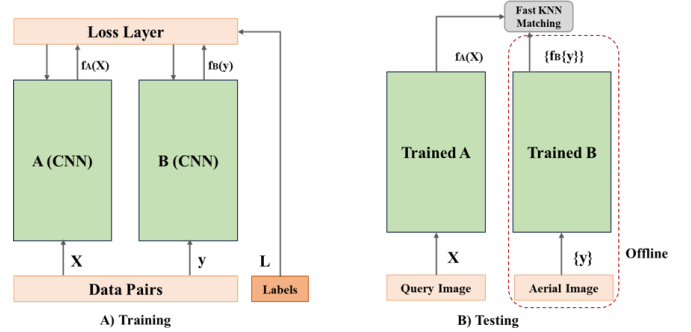


Fig. 7. Lin et al. architecture overview [16].

layers to convert the local features into a shared space before aggregating to get the global descriptor. CVM-Net [17] is notable because the authors combine a Siamese network with NetVALDs layers and learn robust cross-view image representations for matching tasks. In addition, the authors proposed a novel loss called weighted soft margin, which enhances retrieval accuracy and makes the training convergence faster. The results illustrate that CVM-Net-I outperforms CVM-Net-II when AlexNet and VGG-16 are employed as local feature extractors; the accuracy reaches 65.4% and 91.4%, respectively. Furthermore, CVM-Net-I and CVM-Net-II outperform other existing methods [5], [19], [2], and the Siamese network of VGG16 and AlexNet baselines, achieving an accuracy of 67.9% for cropped images and 91.4% for panorama images evaluated on CVUSA and Dayton [19], respectively.

F. Siamese Network-based Models

These models utilize Siamese or triplet network architectures for image-matching tasks between ground-level and aerial/satellite views. They are focused on learning similarity metrics or embeddings to identify matches between images from different viewpoints, emphasizing the importance of capturing semantic and structural similarities across domains.

1) *Where-CNN* [16]: : An early Siamese network [42] inspired the street-view and aerial image matching technique known as Where-CNN. It consists of two CNNs modified from [43] (see Figure 7) having different or identical standard parameters. Regarding different parameters, both learn domain-specific deep representations (called Where-CNN-DS). On the other hand, when parameters are shared, both learn a general representation between aerial and street-view images (called Where-CNN). Moreover, the contrastive loss function proposed in [44] is utilized and is trained using Caffe [45]. The features extracted via Where-CNN and Where-CNN-DS outperform Image-CNN, Places-CNN, and hand-crafted features. Further, Where-CNN-DS, a domain-specific model, achieved slightly better performance than Where-CNN, a domain-independent model. The street view and 45-degree aerial images are collected from Google across seven cities.

G. MLP-based Models

These models are distinguished using Multi-Layer Perceptron (MLP) architectures for aerial-to-street-view generation.

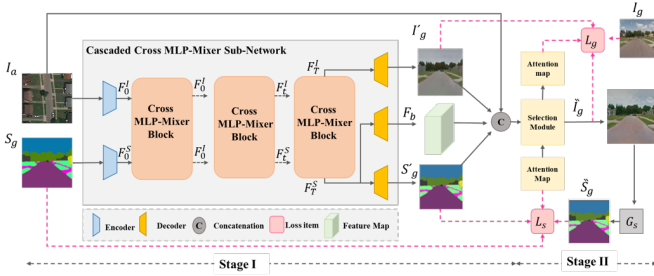


Fig. 8. Ren *et al.* architecture overview [9].

MLPs offer flexibility in capturing complex patterns and relationships within the data, making them suitable for tasks like image synthesis.

1) *CrossMLP* [9]: It is a two-stage framework for aerial-to-street-view generation with a novel cascaded Cross MLP-Mixer (CrossMLP) sub-network as the first stage and a refined pixel loss as the second stage. Figure 8 depicts the overall architecture, wherein the first stage, the Cross-MLP sub-network, stacks multiple Cross-MLP blocks for generating the street view and its corresponding semantic map progressively. Each CrossMLP module captures the structure and appearance information within each view. It can learn the latent correspondence between two inputs by applying a sequential MLP. Then, latent cues guide the transformation from aerial to street view. The refined pixel loss helps with the noisy semantic label by adding more reasonable regularization to the total optimization loss, and with less redundancy, the pixel-level loss becomes more compact. The novelty of this work lies in proposing a two-stage framework for generating street-view images using a novel CrossMLP module. Using CrossMLP to learn the latent mapping cues between aerial-view and street-view semantic maps helps with cross-view translation with accurate appearance and geometry structure. The results showed that CrossMLP performed better than other recent works: Pix2Pix [23], X-Fork [11], X-Seq [11], and SelectionGAN [13], except in terms of PSNR, SD, and SSIM, achieved a bit lower results compared with the others. This study evaluates the method on two benchmark datasets: CVUSA [2] and Dayton [19].

III. DATASETS

We discussed the primary three datasets used for satellite-to-street translation as given in Table II.

Dayton [19]: is introduced for ground-to-aerial or aerial-to-ground image translation or cross-view image synthesis, consisting of 76,048 pairs of satellite and street-view images across 11 different cities in the USA, where 55,000 are reserved for training and the rest for testing. Street-view images are collected from Google Maps of the USA, then several crops are made for each street-view panorama, and for each crop, a satellite image is queried using Google Maps with a resolution of 354×354 . Figure 9 showcases sample images from the dataset.

CVUSA [2]: is an abbreviation of the Crossview United States of America for cross-view geo-localization tasks. The dataset comprises 44,416 satellite and panorama street-view images across the USA, with 35,532 pairs for training and 8,884 for testing. The images are collected from Flickr and Google Street View, having a resolution of 1232×224 . For Flickr, the area has been divided into 100×100 grid; 150 images from each grid cell have been downloaded from 2012 onwards, while the pictures for Google Street View are sampled from randomly selected places within the USA. Moreover, the satellite images are obtained from Bing Maps with a resolution of 750×750 , where for each street-view image, an 800×800 satellite image is downloaded centered on the exact location. Figure 10 showcases sample images from the dataset.

CVACT [18]: stands for Australian Capital Territory City-Scale Cross-View, consisting of 128,334 pairs of satellite and panorama street-view images across Canberra City in Australia. The dataset has 35,532 for training and 92,802 for testing. Street-view images have been collected from the Google Street View API with an image resolution of 1664×832 . The authors have obtained the satellite images from the Google Map API. Further, the matched satellite image at the GPS position has been downloaded for each street-view image with a resolution of 1200×1200 . Figure 11 showcases sample images from the dataset.

IV. EVALUATION METRICS

This section discusses the standard evaluation metrics used in literature for evaluating satellite to street-view generation.

- **Inception Score (IS)**: measures the diversity and quality of the generated images. A good model should produce a reasonable and diverse set of images [46]. The Inception Score is defined as

$$IS = \exp(E_x DKL(p(y|x) || p(y))) \quad (1)$$

Table I shows a few comparative results (i.e., accuracy and inception scores) using Conditional GANs on the CVUSA dataset.

- **Fréchet Inception Distance (FID)**: is based on the extracted visual features and calculates the distance between the actual $p_{real}(x)$ and the generated distribution $p_g(x)$ [46]. As illustrated below, FID computes the multivariate Gaussian for real and generated images.

$$\begin{aligned} FID(p_{real}, p_g) &= d^2((m_{real}, m_g), (m_g, c_g)) \\ &= \|m_{real} - m_g\|^2 + Tr(c_{real} + c_g - 2(c_{real} c_g))^{1/2} \end{aligned} \quad (2)$$

- **Peak Signal to Noise Ratio (PSNR)**: is the ratio between maximum signal power to the distortion noise that affects the signal's ability to be represented accurately [47]. In this case, the ratio between two images is calculated in decibels as expressed.

$$PSNR = 10 \log_{10} \frac{peakval^2}{MSE} \quad (3)$$

TABLE I
QUANTITATIVE COMPARISONS ON THE CVUSA DATASET.

Method	Accuracy (%)				Inception Score			SSIM	PSNR	SD	KL
	Top-1	Top-5	Top-1	Top-5	All	Top-1	Top-5				
Pix2Pix [23]	7.33	9.25	25.81	32.67	3.2771	2.2219	3.4312	0.3923	17.6578	18.523	59.81 ± 2.12
X-Seq [11]	20.58	31.24	50.51	63.66	3.4432	3.5567	3.5567	0.4356	19.0509	18.67	11.71 ± 1.55
X-Fork [11]	15.98	24.14	42.91	54.41	3.8151	2.6738	4.0077	0.4231	18.8067	18.438	15.52 ± 1.73
SelectionGAN [13]	41.52	65.51	74.32	89.66	3.8074	3.9197	3.9197	0.5323	23.1466	19.61	2.96 ± 0.97
CrossMLP [9]	44.96	69.96	76.98	91.91	3.8392	2.8035	3.9757	0.5251	23.1532	19.58	2.69 ± 0.94
Real Data	7	-	-	-	4.8741	3.2959	4.9943	-	-	-	-

TABLE II
SUMMARY OF THE DATASETS USED FOR SATELLITE TO STREET VIEW TRANSLATION.

Dataset	Year	Ground-View FoV	GPS-tag	Resolution		Training	Images Testing	Total
				Images	Satellite			
Dayton	2016	-	-	354×354	354×354	55,000	21,048	76,048
CVUSA	2017	360	No	1232×224	750×750	35,532	8,884	44,416
CVACT	2019	360	Yes	1664×832	1200×1200	35,532	92,802	128,334



Fig. 9. sample street-view and satellite image pair from Dayton dataset.



Fig. 10. Sample street-view and satellite image pair from CVUSA dataset.

- **Structure Similarity Index Method (SSIM):** determines the similarity between the original image and its recovered version. In SSIM, the degradation of images is considered an alteration in how structural information is perceived. Additionally, it collaborates with other key perception-based facts like contrast masking (contrast masking is a process where the degree of distortion is less apparent in the image's texture) and luminance masking (a process where distortion is less clear at image boundaries). The SSIM is expressed in terms of contrast, luminance, and structure as follows

$$SSIM(x, y) = [l(x, y)]^\alpha \cdot [c(x, y)]^\beta \cdot [s(x, y)]^\gamma. \quad (4)$$

The luminance, contrast and structure are expressed as

$$\begin{aligned} l(x, y) &= \frac{2\mu_x\mu_y + C_1}{\mu_x^2 + \mu_y^2 + C_1}, \\ c(x, y) &= \frac{2\sigma_x\sigma_y + C_2}{\sigma_x^2 + \sigma_y^2 + C_2}, \\ s(x, y) &= \frac{\sigma_{xy} + C_3}{\sigma_x\sigma_y + C_3}. \end{aligned} \quad (5)$$

- **Kullback–Leibler (KL) divergence:** estimates the similarity of the probability distribution between the real and generated images [48]. The zero KL value refers to an identical distribution, while the higher KL value refers to less similarity [49] between the images. The KL divergence can be calculated as follows.



Fig. 11. Sample street-view and satellite image pair from CVACT dataset.

$$KL(p \parallel q) = E_x[\log(\frac{p(x)}{q(x)})]. \quad (6)$$

V. CHALLENGES, LIMITATIONS AND FUTURE DIRECTIONS

The following sections highlight the challenges and limitations in the Satellite to Street View generation with possible future directions.

Limited available datasets: The datasets for synthesizing street-view from satellite images are limited in number and not publicly available; they need to be requested from their corresponding authors. This hinders progress; making publicly available datasets will help deliver good-quality research and engage the research community.

High computational cost: Despite the success of recent deep learning methods in training huge models, they require a lot of training data to learn the modality-specific rules or find the relation between the various objects on their own. As a result, it requires a longer training time, a considerable amount of training data, and high computational requirements compared with CNN [50]. It should be noted that satellite-to-street-view generation requires more data as the relation is very complex due to the entirely different input and output in terms of viewpoint.

Evaluation metrics: Finding appropriate and more specific evaluation metrics for this type of task is challenging. The evaluation metrics applied in the literature, like inception scores, PSNR, SSIM, and SD, are generally for image quality, not specifically for image synthesizing for under-consideration tasks.

Lack of multi-modalities: Using a single data modality depending on a single image, like a satellite image, for generating street view is more challenging than using multiple data modalities. However, some of the recent works [12], [13] rely on some auxiliary information like segmentation maps for generating street-view. Regardless, generating segmentation maps may limit the methods if there is any difficulty with its computation, affecting the quality of the synthesized street-view image. Multi-modal datasets might solve the problem and increase the quality of the generation.

Low-resolution layout images: The satellite images are taken from very far away, only harboring the building’s rooftops with little or no information about small objects like building facades. In addition, many local details, such as vehicles and pedestrians, are not captured in satellite images, which makes

it difficult to consider these objects during street view synthesis. Also, in satellite images, places with similar street layouts might appear completely different in the street view, which results in less variation in the synthesized street view images. Moreover, due to the high similarity between road textures and other materials like buildings’ roofs, it is sometimes difficult to distinguish road layouts from buildings’ roofs. To overcome these limitations, images must be taken from a reasonable height containing as much information about the object as possible to help synthesize views true to its street view.

Lack of novel techniques: The methods used in the literature need to be updated; currently, generative adversarial network and their variants are the most popular choices for a street-view generation. Moreover, various CNNs are employed for feature extraction, while Siamese and Triplet Networks have been used for street-view geo-localization tasks. Researchers must consider and focus on recent state-of-the-art techniques such as transformers and stable diffusion for satellite to street-view synthesizing.

Image quality degradations: The satellite image clarity and quality are usually affected by atmospheric conditions, illumination conditions, and noise. Similarly, the satellite images may also be obscured due to dust and clouds, significantly affecting the quality of the generated street-view images. In some cases, building and tree shadows affect the satellite image clarity, which causes the street layouts to be difficult to recognize. One way to solve the mentioned problem is by adopting shadow removal techniques; although these might be useful, but they will have computational costs.

Diverse weather conditions: In usual image generation techniques, the conditions are generally constant and do not change over the course. However, for this task, the same image may have to be generated under diverse conditions, such as the exact layout being different for day and night, snow and spring seasons and many others. This situation needs to have representative images in the datasets to be created.

VI. CONCLUSION

This paper has surveyed the satellite to street-view synthesis domain from different aspects, including the recently available methods, common datasets (benchmark datasets), common evaluation metrics, and challenges and limitations, by examining 20 recently published papers. It is clear from reviewed papers that the Generative Neural Network (GAN) and its varieties are very immersed and widely used in this

domain, despite other novel methods are available. Also, despite the success of the review methods, the methods in the literature still failed to generate small and detailed objects, which confirms that novel and updated methods need to be used for synthesizing more realistic and detailed street-view images. Along with this, a limited number of datasets have been used in the majority of the surveyed papers in this domain, which indicates the need for more publicly available datasets to enrich the research in this domain. In addition, more specific evaluation metrics need to be investigated and applied in this domain, as the methods in the literature have been evaluated on image quality-based metrics. Overall, the disclosed research challenges highlight that the satellite to street-view synthesis is still an active area of research.

REFERENCES

- [1] X. Lu, Z. Li, Z. Cui, M. R. Oswald, M. Pollefeys, and R. Qin, "Geometry-aware satellite-to-ground image synthesis for urban areas," in *Proceedings of the IEEE/CVF Conference on Computer Vision and Pattern Recognition*, 2020, pp. 859–867. [1](#), [2](#), [3](#), [4](#)
- [2] S. Workman, R. Souvenir, and N. Jacobs, "Wide-area image geolocalization with aerial reference imagery," in *Proceedings of the IEEE International Conference on Computer Vision*, 2015, pp. 3961–3969. [1](#), [3](#), [4](#), [5](#), [6](#), [7](#), [8](#)
- [3] D. J. Crandall, L. Backstrom, D. Huttenlocher, and J. Kleinberg, "Mapping the world's photos," in *Proceedings of the 18th international conference on World wide web*, 2009, pp. 761–770. [1](#)
- [4] A. Toker, Q. Zhou, M. Maximov, and L. Leal-Taixé, "Coming down to earth: Satellite-to-street view synthesis for geo-localization," in *Proceedings of the IEEE/CVF Conference on Computer Vision and Pattern Recognition*, 2021, pp. 6488–6497. [1](#), [5](#), [6](#)
- [5] M. Zhai, Z. Bessinger, S. Workman, and N. Jacobs, "Predicting ground-level scene layout from aerial imagery," in *Proceedings of the IEEE Conference on Computer Vision and Pattern Recognition*, 2017, pp. 867–875. [1](#), [3](#), [4](#), [5](#), [6](#), [7](#)
- [6] X. Deng, Y. Zhu, and S. Newsam, "What is it like down there? generating dense ground-level views and image features from overhead imagery using conditional generative adversarial networks," in *Proceedings of the 26th ACM SIGSPATIAL International Conference on Advances in Geographic Information Systems*, 2018, pp. 43–52. [1](#), [3](#)
- [7] Y. Shi, D. Campbell, X. Yu, and H. Li, "Geometry-guided street-view panorama synthesis from satellite imagery," *IEEE Transactions on Pattern Analysis and Machine Intelligence*, vol. 44, no. 12, pp. 10009–10022, 2022. [1](#), [5](#), [6](#)
- [8] S. Wu, H. Tang, X.-Y. Jing, J. Qian, N. Sebe, Y. Yan, and Q. Zhang, "Cross-view panorama image synthesis with progressive attention gans," *Pattern Recognition*, vol. 131, p. 108884, 2022. [1](#), [4](#), [5](#)
- [9] B. Ren, H. Tang, and N. Sebe, "Cascaded cross mlp-mixer gans for cross-view image translation," *arXiv preprint arXiv:2110.10183*, 2021. [1](#), [8](#), [9](#)
- [10] O. Ronneberger, P. Fischer, and T. Brox, "U-net: Convolutional networks for biomedical image segmentation," in *Medical Image Computing and Computer-Assisted Intervention—MICCAI 2015: 18th International Conference, Munich, Germany, October 5–9, 2015, Proceedings, Part III 18*. Springer, 2015, pp. 234–241. [1](#), [2](#), [4](#), [5](#)
- [11] K. Regmi and A. Borji, "Cross-view image synthesis using conditional gans," in *Proceedings of the IEEE conference on Computer Vision and Pattern Recognition*, 2018, pp. 3501–3510. [1](#), [2](#), [3](#), [4](#), [5](#), [6](#), [8](#), [9](#)
- [12] H. Tang, D. Xu, Y. Yan, P. H. Torr, and N. Sebe, "Local class-specific and global image-level generative adversarial networks for semantic-guided scene generation," in *Proceedings of the IEEE/CVF Conference on Computer Vision and Pattern Recognition (CVPR)*, June 2020. [1](#), [4](#), [5](#), [10](#)
- [13] H. Tang, D. Xu, N. Sebe, Y. Wang, J. J. Corso, and Y. Yan, "Multi-channel attention selection gan with cascaded semantic guidance for cross-view image translation," in *Proceedings of the IEEE/CVF conference on computer vision and pattern recognition*, 2019, pp. 2417–2426. [1](#), [4](#), [5](#), [8](#), [9](#), [10](#)
- [14] K. Regmi and M. Shah, "Bridging the domain gap for ground-to-aerial image matching," in *Proceedings of the IEEE/CVF International Conference on Computer Vision*, 2019, pp. 470–479. [1](#), [2](#), [3](#), [6](#)
- [15] Y. Shi, X. Yu, D. Campbell, and H. Li, "Where am i looking at? joint location and orientation estimation by cross-view matching," in *Proceedings of the IEEE/CVF Conference on Computer Vision and Pattern Recognition*, 2020, pp. 4064–4072. [1](#), [6](#)
- [16] T.-Y. Lin, Y. Cui, S. Belongie, and J. Hays, "Learning deep representations for ground-to-aerial geolocalization," in *Proceedings of the IEEE Conference on Computer Vision and Pattern Recognition (CVPR)*, June 2015. [1](#), [7](#)
- [17] S. Hu, M. Feng, R. M. Nguyen, and G. H. Lee, "Cvm-net: Cross-view matching network for image-based ground-to-aerial geo-localization," in *Proceedings of the IEEE Conference on Computer Vision and Pattern Recognition*, 2018, pp. 7258–7267. [1](#), [3](#), [6](#), [7](#)
- [18] L. Liu and H. Li, "Lending orientation to neural networks for cross-view geo-localization," in *Proceedings of the IEEE/CVF Conference on Computer Vision and Pattern Recognition (CVPR)*, June 2019. [1](#), [6](#), [7](#), [8](#)
- [19] N. N. Vo and J. Hays, "Localizing and orienting street views using overhead imagery," in *Computer Vision—ECCV 2016: 14th European Conference, Amsterdam, The Netherlands, October 11–14, 2016, Proceedings, Part I 14*. Springer, 2016, pp. 494–509. [1](#), [2](#), [3](#), [4](#), [6](#), [7](#), [8](#)
- [20] A. Swerdlow, R. Xu, and B. Zhou, "Street-view image generation from a bird's-eye view layout," *IEEE Robotics and Automation Letters*, 2024. [2](#), [3](#)
- [21] H. Caesar, V. Bankiti, A. H. Lang, S. Vora, V. E. Liong, Q. Xu, A. Krishnan, Y. Pan, G. Baldan, and O. Beijbom, "nusenes: A multimodal dataset for autonomous driving," in *Proceedings of the IEEE/CVF conference on computer vision and pattern recognition*, 2020, pp. 11 621–11 631. [2](#)
- [22] J.-Y. Zhu, R. Zhang, D. Pathak, T. Darrell, A. A. Efros, O. Wang, and E. Shechtman, "Toward multimodal image-to-image translation," *Advances in neural information processing systems*, vol. 30, 2017. [2](#)
- [23] P. Isola, J.-Y. Zhu, T. Zhou, and A. A. Efros, "Image-to-image translation with conditional adversarial networks," in *Proceedings of the IEEE conference on computer vision and pattern recognition*, 2017, pp. 1125–1134. [2](#), [3](#), [4](#), [5](#), [6](#), [8](#), [9](#)
- [24] X. Zhu, Z. Yin, J. Shi, H. Li, and D. Lin, "Generative adversarial frontal view to bird view synthesis," in *2018 International conference on 3D Vision (3DV)*. IEEE, 2018, pp. 454–463. [3](#), [5](#)
- [25] J.-Y. Zhu, T. Park, P. Isola, and A. A. Efros, "Unpaired image-to-image translation using cycle-consistent adversarial networks," in *Proceedings of the IEEE international conference on computer vision*, 2017, pp. 2223–2232. [3](#)
- [26] T. Kim, M. Cha, H. Kim, J. K. Lee, and J. Kim, "Learning to discover cross-domain relations with generative adversarial networks," in *International conference on machine learning*. PMLR, 2017, pp. 1857–1865. [3](#)
- [27] M.-Y. Liu and O. Tuzel, "Coupled generative adversarial networks," *Advances in neural information processing systems*, vol. 29, 2016. [3](#)
- [28] A. Palazzi, G. Borghi, D. Abati, S. Calderara, and R. Cucchiara, "Learning to map vehicles into bird's eye view," in *Image Analysis and Processing-ICIAP 2017: 19th International Conference, Catania, Italy, September 11–15, 2017, Proceedings, Part I 19*. Springer, 2017, pp. 233–243. [3](#)
- [29] S. Ardeshir and A. Borji, "Ego2top: Matching viewers in egocentric and top-view videos," in *Computer Vision—ECCV 2016: 14th European Conference, Amsterdam, The Netherlands, October 11–14, 2016, Proceedings, Part V 14*. Springer, 2016, pp. 253–268. [4](#)
- [30] M. Cordts, M. Omran, S. Ramos, T. Rehfeld, M. Enzweiler, R. Benenson, U. Franke, S. Roth, and B. Schiele, "The cityscapes dataset for semantic urban scene understanding," in *Proceedings of the IEEE conference on computer vision and pattern recognition*, 2016, pp. 3213–3223. [4](#)
- [31] J.-Y. Zhu, P. Krähenbühl, E. Shechtman, and A. A. Efros, "Generative visual manipulation on the natural image manifold," in *Computer Vision—ECCV 2016: 14th European Conference, Amsterdam, The Netherlands, October 11–14, 2016, Proceedings, Part V 14*. Springer, 2016, pp. 597–613. [4](#)
- [32] A. Yu and K. Grauman, "Fine-grained visual comparisons with local learning," in *Proceedings of the IEEE conference on computer vision and pattern recognition*, 2014, pp. 192–199. [4](#)
- [33] M. Eitz, J. Hays, and M. Alexa, "How do humans sketch objects?" *ACM Transactions on graphics (TOG)*, vol. 31, no. 4, pp. 1–10, 2012. [4](#)
- [34] P.-Y. Laffont, Z. Ren, X. Tao, C. Qian, and J. Hays, "Transient attributes for high-level understanding and editing of outdoor scenes," *ACM Transactions on graphics (TOG)*, vol. 33, no. 4, pp. 1–11, 2014. [4](#)

- [35] A. Radford, L. Metz, and S. Chintala, "Unsupervised representation learning with deep convolutional generative adversarial networks," *arXiv preprint arXiv:1511.06434*, 2015. [4](#)
- [36] S. Ioffe and C. Szegedy, "Batch normalization: Accelerating deep network training by reducing internal covariate shift," in *International conference on machine learning*. pmlr, 2015, pp. 448–456. [4](#)
- [37] R. Zhang, P. Isola, and A. A. Efros, "Colorful image colorization," in *Computer Vision—ECCV 2016: 14th European Conference, Amsterdam, The Netherlands, October 11–14, 2016, Proceedings, Part III 14*. Springer, 2016, pp. 649–666. [4](#)
- [38] A. Bansal, X. Chen, B. Russell, A. Gupta, and D. Ramanan, "Pixelnet: Towards a general pixel-level architecture," *arXiv preprint arXiv:1609.06694*, 2016. [5](#)
- [39] X. Glorot and Y. Bengio, "Understanding the difficulty of training deep feedforward neural networks," in *Proceedings of the thirteenth international conference on artificial intelligence and statistics*. JMLR Workshop and Conference Proceedings, 2010, pp. 249–256. [5](#)
- [40] S. Workman and N. Jacobs, "On the location dependence of convolutional neural network features," in *Proceedings of the IEEE Conference on Computer Vision and Pattern Recognition Workshops*, 2015, pp. 70–78. [5](#)
- [41] B. Zhou, A. Lapedriza, J. Xiao, A. Torralba, and A. Oliva, "Learning deep features for scene recognition using places database," *Advances in neural information processing systems*, vol. 27, 2014. [5](#)
- [42] S. Chopra, R. Hadsell, and Y. LeCun, "Learning a similarity metric discriminatively, with application to face verification," in *2005 IEEE Computer Society Conference on Computer Vision and Pattern Recognition (CVPR'05)*, vol. 1. IEEE, 2005, pp. 539–546. [7](#)
- [43] A. Krizhevsky, I. Sutskever, and G. E. Hinton, "Imagenet classification with deep convolutional neural networks," *Communications of the ACM*, vol. 60, no. 6, pp. 84–90, 2017. [7](#)
- [44] R. Hadsell, S. Chopra, and Y. LeCun, "Dimensionality reduction by learning an invariant mapping," in *2006 IEEE Computer Society Conference on Computer Vision and Pattern Recognition (CVPR'06)*, vol. 2. IEEE, 2006, pp. 1735–1742. [7](#)
- [45] Y. Jia, E. Shelhamer, J. Donahue, S. Karayev, J. Long, R. Girshick, S. Guadarrama, and T. Darrell, "Caffe: Convolutional architecture for fast feature embedding," in *Proceedings of the 22nd ACM international conference on Multimedia*, 2014, pp. 675–678. [7](#)
- [46] S. S. Baraheem, T.-N. Le, and T. V. Nguyen, "Image synthesis: a review of methods, datasets, evaluation metrics, and future outlook," *Artificial Intelligence Review*, pp. 1–53, 2023. [8](#)
- [47] U. Sara, M. Akter, and M. S. Uddin, "Image quality assessment through fsim, ssim, mse and psnr—a comparative study," *Journal of Computer and Communications*, vol. 7, no. 3, pp. 8–18, 2019. [8](#)
- [48] E. Betzalel, C. Penso, A. Navon, and E. Fetaya, "A study on the evaluation of generative models," *arXiv e-prints*, pp. arXiv–2206, 2022. [9](#)
- [49] A. Solanki, A. Nayyar, and M. Naved, *Generative Adversarial Networks for Image-to-Image Translation*. Academic Press, 2021. [9](#)
- [50] S. Khan, M. Naseer, M. Hayat, S. W. Zamir, F. S. Khan, and M. Shah, "Transformers in vision: A survey," *ACM computing surveys (CSUR)*, vol. 54, no. 10s, pp. 1–41, 2022. [10](#)